An Evaluation of Antarctic Sea-Ice Thickness from the Global Ice-Ocean Modeling and Assimilation System based on In situ and Satellite Observations

Sutao Liao[1], Hao Luo[1*], Jinfei Wang[1], Qian Shi[1], Jinlun Zhang[2], Qinghua Yang[1]

[1]School of Atmospheric Sciences, Sun Yat-sen University, and Southern Marine Science and Engineering Guangdong Laboratory (Zhuhai), Zhuhai, 519082, China

[2]Polar Science Center, Applied Physics Lab, University of Washington, Seattle, WA 98105

Correspondence to: Hao Luo (luohao25@mail.sysu.edu.cn)

Abstract. Antarctic sea ice is an important component of the Earth system. However, its role in the Earth system is still unclear due to limited Antarctic sea-ice thickness (SIT) data. A reliable sea-ice reanalysis can be useful to study Antarctic SIT and its role in the Earth system. Among various Antarctic sea-ice reanalyses products, the Global Ice-Ocean Modeling and Assimilation System (GIOMAS) output is widely used in the researches of Antarctic sea ice. As more Antarctic SIT observations with quality control are released, a further evaluation of Antarctic SIT from GIOMAS is conducted in this study based on in situ and satellite observations. Generally, though only sea-ice concentration is assimilated, GIOMAS can basically reproduce the observed variability of sea-ice volume and its changes in the trend before and after 2013, indicating that GIOMAS is a good option to study the long-term variation of Antarctic sea ice. However, due to deficiencies in the model and asymmetric changes in SIT caused by assimilation, GIOMAS underestimates Antarctic SIT especially in deformed ice regions, which has an impact on not only the mean state of SIT but also the variability. Thus, besides the further development of the model, assimilating additional sea-ice observations (e.g., SIT and sea-ice drift) with advanced assimilation methods may be conducive to a more accurate estimation of Antarctic SIT.

1   Introduction

Antarctic sea ice plays an important role in the Earth system. Firstly, Antarctic sea ice can influence the Earth climate system. For instance, changes in Antarctic sea ice could affect freshwater flux of the

26   Southern Ocean that directly influences the stratification of the ocean (Goosse and Zunz, 2014; Haumann

27   et al., 2016). Besides, Antarctic sea ice acts as a protective buffer for Antarctic ice shelves, with the

28   thinning or absence of sea ice increasing the possibility of ice shelf disintegration (Robel, 2017; Massom

29   et al., 2018). Secondly, Antarctic sea ice has a significant impact on the biosphere of the Earth system.

30   Studies have shown that the variation of Antarctic sea-ice thickness (SIT) will affect the maximum

31   biomass of algae in different ice layers, which will influence the food web of the Southern Ocean

32   (Massom and Stammerjohn, 2010; Schultz, 2013). Thirdly, Antarctic sea ice has impacts on human

33   activities such as shipping and fishery management (Dahood et al., 2019; Mishra et al., 2021). Hence,

34   studies on Antarctic sea ice are of great scientific and socio-economic importance.

35   To truly understand changes in sea ice of the Southern Ocean, SIT is needed to estimate the sea-ice

36   volume (SIV), since it is through volume changes that sea ice has its greatest impact on the water column

37   (Maksym et al., 2012; Hobbs et al., 2016). Although changes in Antarctic sea-ice extent (SIE) have been

38   investigated extensively (Turner et al., 2015; Parkinson, 2019), they may not be a robust proxy of large-

39   scale changes in SIV as there are differences between the variation of SIV and SIE in some regions of

40   the Antarctic (e.g., Kurtz and Markus, 2012). Many studies related to Antarctic sea ice are limited by the

41   lack of reliable SIT data. For example, freshwater flux of the Southern Ocean, which affects the

42   stratification of ocean, cannot be accurately estimated as part of the freshwater flux comes from sea-ice

43   melting and growth (Haumann et al., 2016). In addition, the skill of sea-ice prediction cannot meet the

44   need of human activities in the Antarctic (Mishra et al., 2021). Studies have shown that the skill of

45   Antarctic sea-ice prediction could be improved with better SIT initialization (Bushuk et al., 2021). So

46   far, the commonly used types of the Antarctic SIT data are observations, model data, and reanalyses

47   products and each type of data has its own limitations.

48   Antarctic SIT observations can be divided into in situ and satellite observations. In situ observations can

49   provide the local state of Antarctic SIT. However, the sparse distribution of in situ SIT observations pose

50   considerable challenges to understand the large-scale characteristics of SIT (Worby et al., 2008a). It is

51   well known that satellite observations have wider spatiotemporal coverage than in situ observations.

52   However, previous studies indicate that there is large uncertainty in SIT data retrieval from satellite

53   altimeters owing to the relatively small freeboard (i.e., thickness of sea ice or sea ice and snow above the

54   sea surface) of Antarctic sea ice compared to that in the Arctic (Maksym and Markus, 2008) and the lack

55   of knowledge about coincident snow cover thickness as well as sea ice and snow density (Alexandrov et

al., 2010). In addition, results of numerical simulations are used to investigate the long-term variation of Antarctic SIT (Zhang, 2007; Holland et al., 2014), but discrepancies are identified not only between models and observations but also among models (Shu et al., 2015; Tsujino et al., 2020), indicating the large uncertainty in model estimates.

It should be noted that reanalyses have unique advantages over observed and simulated SIT. Theoretically, reanalyses can provide more accurate or comprehensive state estimations than can otherwise be obtained through either observations or models alone (Buehner et al., 2017). Reanalyses merges the information from both observations and models through data assimilation. Compared with observations, reanalyses data can provide coordinated and gridded data with homogenous sampling in time and space over a long period (Parker, 2016). Besides, compared with model only data, reanalyses data can produce the state estimations closer to observations because of data assimilation (Lindsay and Zhang, 2006; Rollenhagen et al., 2009). Hence, SIT reanalyses have been widely adopted in studies on the Antarctic sea ice (Abernathey et al., 2016; Kumar et al., 2017). Nevertheless, there are still large uncertainties of present sea-ice reanalyses in the Southern Ocean (Uotila et al., 2019; Shi et al., 2021), suggesting the necessity and importance of evaluating them.

Among a number of Antarctic sea-ice reanalyses, the Global Ice-Ocean Modeling and Assimilation System (GIOMAS) is one of the most widely used in studies of Antarctic sea ice. For instance, GIOMAS has been regarded as the reference in the assessments of simulations (Shu et al., 2015; Uotila et al., 2017; DuVivier et al., 2020) and predictions (Ordoñez et al., 2018; Morioka et al., 2021). However, GIOMAS has been less widely evaluated, in part because there are far fewer observations of Antarctic SIT against which evaluation is possible (DuVivier et al., 2020).

Due to advances in observing technology as well as algorithms in recent years, the quality of Antarctic SIT observations is improved. For example, compared to the European Remote-Sensing Satellites (i.e., ERS-1 and ERS-2), the Synthetic-Aperture Interferometric Radar Altimeter (SIRAL) on board CryoSat-2 (CS2) is equipped with two radar antennas, which significantly improves the accuracy of sea-ice freeboard (i.e., thickness of sea ice above the sea surface). CS2 also has a much wider spatial coverage with improved along-track resolution because of the design of the satellite orbit and multiple operation modes (Parrinello et al., 2018). In addition, Paul et al. (2018) developed an adaptive retracker threshold for CS2 to produce a consistent sea-ice freeboard data. Besides, more Antarctic SIT observations has been available with the accumulation of observations. For instance, more in situ observations are

86 obtained from dedicated research stations, icebreakers and autonomous underwater vehicles due to

87 increasing research activities in the Antarctic. These provide an opportunity to further evaluate Antarctic

88 SIT of GIOMAS. Notably, since in situ observations provide relatively accurate estimations in specific

89 points while satellite data provides relatively long and continuous observations with wide spatial

90 coverage, various observations are adopted in the evaluation to make it more comprehensive.

91 The paper is organized as follows. In Sect. 2, Antarctic SIT from GIOMAS and observations are

92 introduced. In Sect. 3, Antarctic SIT of GIOMAS is evaluated with observations from different aspects,

93 including the climatology, the linear trend, the intensity of variability, as well as the frequency

94 distribution. The final section provides the conclusions and discussion.

95 **2   Data and methods**

96 **2.1   SIT from GIOMAS**

97 GIOMAS consists of a global Parallel Ocean and sea Ice Model (POIM) with data assimilation

98 capabilities, which is developed at University of Washington (Zhang and Rothrock, 2003). The ocean

99 component of POIM is the Parallel Ocean Program, and the sea-ice component of POIM is the 8-category

100 thickness and enthalpy distribution sea-ice model. The National Centres for Environmental Prediction-

101 National Centre for Atmospheric Research (NCEP-NCAR) daily reanalysis (Kalnay et al., 1996)

102 provides the atmospheric forcing for POIM. Furthermore, in GIOMAS, the modelled sea-ice

103 concentration (SIC) is nudged towards observed SIC derived from Special Sensor Microwave Imager

104 launched by the Defense Meteorological Satellite Program (Weaver et al., 1987), and other modelled

105 variables including SIT are adjusted subsequently. The detailed adjustment process of SIT is as follows:

106 when SIC is nudged in the system, it will modify the SIT distribution to accommodate the change in SIC,

107 which remove sea ice from the distribution without considering its SIT if modelled SIC is too large, while

108 add sea ice to the 0.1-m ice thickness bin if modelled SIC is too small. (Lindsay and Zhang, 2006). This

109 process can reduce the root-mean-square difference and improve the correlation between modelled SIT

110 and observed SIT and will also cause the thinning of the mean SIT. More technical details for POIM and

111 assimilation procedures can be found in Zhang and Rothrock (2003) and Lindsay and Zhang (2006),

112 respectively. GIOMAS data is available from 1979 to the present with a global coverage and data

113 involved in the assessment spans from January 1979 to December 2018 (Fig. 1a). The average horizontal

spatial resolution is 0.8 degrees of longitude × 0.8 degrees of latitude (around 60 km × 60 km), and the temporal resolution is one month for all variables. Additionally, GIOMAS also provides daily outputs for some variables including SIT, SIC and snow depth, and the daily SIT of GIOMAS is assessed in this study. SIT data of GIOMAS is the equivalent SIT, which represents SIV per unit area.

2.2　SIT from satellite altimeters and in situ observations

Satellite-altimeter observations involved in this study are from radar altimeters on board Envisat (ES) and CS2, which are generated by the Sea Ice Climate Change Initiative (SICCI) project under the European Space Agency Climate Change Initiative (ESA CCI) program. ES was equipped with the Radar Altimeter 2, measuring sea-ice freeboard mainly based on K_u-band frequency (Hendricks et al., 2018b). The Antarctic SIT data derived from ES freeboard spans from December 2002 to November 2011 (Fig. 1a) with a coverage of the entire Antarctica (Fig. 1b). The spatial resolution is 50 km × 50 km and the temporal resolution is 1 month. CS2 was equipped with the SIRAL, measuring the sea-ice freeboard mainly based on K_u-band frequency like ES (Hendricks et al., 2018a). CS2 Antarctic SIT dataset spans from November 2010 to April 2017 (Fig. 1a) and the spatial coverage and the spatiotemporal resolution are the same as ES SIT dataset.

In situ SIT observations involved in this study are from upward looking sonar (ULS), ship-based and air-based measurements. ULS is a kind of mooring measurement at fixed locations, measuring sea-ice draft (thickness of sea ice below the water surface) with a time interval shorter than 15 minutes (Behrendt et al., 2013). Ice draft needs to be converted into total SIT in an empirical way according to Harms et al. (2001). Thirteen ULSs used in this study were deployed in the Weddell Sea (Fig. 1b) by Alfred Wegener Institute (AWI) and spanned from 1990 to 2010 intermittently (Fig. 1a).

The ship-based observations are made up of the Antarctic Sea Ice Processes & Climate program (ASPeCt), ANT-XXIX/6 (Schwegmann, 2013) and ANT-XXIX/7 (Ricker, 2016). The ASPeCt dataset not only includes ASPeCt observations collected from 1981 to 2005 (Worby et al., 2008a), but also includes the ASPeCt bridge-based sea-ice observations collected from 2007 to 2012. The ship tracks cover all sectors of the Southern Ocean (Fig. 1b) and the average spacing of data points is 6 nautical miles. The air-based SIT observations include data collected by the air-based electromagnetic system (i.e., like an electromagnetic bird carried by the helicopter) with a high frequency of 0.5 Hz and an

142 average spacing of 3-4 m (Lemke, 2009, 2014), which is mainly located in the northwest Weddell Sea

143 (Fig. 1b).

144 Since both satellite observations and in situ observations are involved in the evaluation, it is necessary

145 to investigate the relationship between them. To achieve this, direct comparisons among satellite

146 observations and ULS observations are conducted in the Weddell Sea where ULS SIT observations are

147 available. The monthly SIT of ES and CS2 during their coincident segments (i.e., November 2010 to

148 November 2011) in the Weddell Sea is displayed in Fig. 2a. The SIT of ES and CS2 is mainly distributed

149 around the one-to-one line and there is a significant correlation of 0.69 between them, indicating ES-

150 derived SIT is comparable to CS2-derived SIT. Then the monthly ES SIT is compared with monthly

151 ULS SIT during the coincident segments at sites 206, 207, 208, 229, 231 and 233 (Fig. 2b). CS2 dataset

152 is not involved since there are only four data pairs between CS2 and ULS observations. The distribution

153 of data pairs indicates ES tends to overestimate SIT compared with ULS observations, because the

154 scattering surface of the radar altimeter can be inside the snow (Willatt et al., 2010; Wang et al., 2020).

155 However, 77% of ULS SIT is within the uncertainty of ES (Fig. 2b). Besides, the correlation between

156 the ULS SIT that is within the uncertainty of ES and the corresponding ES SIT is 0.73. All those indicate

157 ES-derived SIT is comparable to ULS observations when the uncertainty is considered.

158

159 **2.3   Data processing and methods**

160 According to Parkinson and Cavalieri (2012), the summer, autumn, winter and spring refer to January-

161 March, April-June, July-September and October-December, respectively. As shown in Fig. 2b, the

162 Southern Ocean is divided into the Weddell Sea (60° W-20° E), the Indian Ocean (20° E-90°E), the

163 western Pacific Ocean (90°E-160°E), the Ross Sea (160°E-130°W) and the Amundsen/Bellingshausen

164 Sea (130°W-60°W).

165 Since the mismatch in spatial and temporal resolutions between reanalyses and observations could

166 introduce substantial representation errors in the comparisons, the data is processed as Janjić et al. (2018)

167 suggested to eliminate such mismatch between GIOMAS and observations. In general, GIOMAS data is

168 converted to the locations of the observations when compared with satellite and ULS observations while

169 the ship-based and air-based observations are converted to gridded data based on GIOMAS grid. For

170 details, when compared with satellite observations, daily GIOMAS data is interpolated to the grid of

171   satellite observations using the linear approach and converted to monthly averages. For the comparisons

172   between GIOMAS and ULS observations, 15-minutely ULS data is converted to daily averages for

173   comparison with daily GIOMAS data and the nearest neighbour approach is used to find the GIOMAS

174   grid cells closest to the ULS locations. Besides, when compared with ship-based and air-based

175   observations, since the observed data is very dense in space and the temporal resolution is always within

176   one day, it is averaged into daily and gridded data based on the GIOMAS grid to create a proper dataset

177   that is compatible with daily GIOMAS SIT data.

178   The climatological annual cycle is defined as the multi-year averages in each month. For observations,

179   the climatological annual cycles are calculated from all years available in each observation dataset. For

180   GIOMAS, when compared with satellite observations, GIOMAS data that coincides with the time spans

181   of satellite observations are selected (2002-2011 for ES and 2010-2017 for CS2) to calculate the

182   climatology. When compared with ULS observations, all years available in GIOMAS (1979-2018) are

183   used for the computation of climatology. Anomalies are defined as departures from the climatological

184   annual cycle, and the intensity of variability is defined as the standard deviation of anomalies. During

185   the overlapping time of ES and CS2 (November 2010 to November 2011), though the difference in SIV

186   anomalies between ES and CS2 (i.e., root-mean-square error is 473.1 km^3) is not small compared with

187   the mean standard deviation of SIV anomalies (i.e., their standard deviations in ES and CS2 are 960.7

188   km^3 and 956.6 km^3, respectively), the selection of data in the coincident segment has little effect on the

189   trend. Thus, the SIV anomalies of CS2 during the overlapping time are chosen and ES from December

190   2002 to October 2010 and CS2 from November 2010 to April 2017 are combined to obtain a relatively

191   long and continuous SIV time series for the trend computation. In addition, since the trajectories of air-

192   based SIT observations are mainly distributed in the northwest Weddell Sea where is dominated by

193   deformed sea ice (Fig. 2b), the comparison between GIOMAS and air-based observations is only

194   conducted in the Weddell Sea.

195   **3   Results**

196   **3.1   Comparison in the climatology of SIV and SIT**

197   Figure 3 shows the climatological annual cycle of Antarctic SIV. Although obvious uncertainties of SIV

198   can be found in both ES and CS2, the annual cycle of ES is similar to that of CS2. Both ES and CS2

199 show that the melt rate of sea ice is nearly twice the growth rate. Besides, there are also some differences

200 in the SIV climatology between ES and CS2. The SIV of CS2 is greater than that of ES in the winter and

201 spring, and larger uncertainties of SIV can be found in ES. The SIV difference between ES and CS2 may

202 be owing to the mismatch in the sea-ice freeboard between ES and CS2. As Paul et al. (2018) indicated,

203 due to the unresolved physical processes such as complex snow metamorphism or sea-ice surface

204 roughness influenced by the flooding in the snow/ice interface, the sea-ice freeboard of ES cannot be

205 well matched with the ones of CS2 in the Antarctic though the retracker algorithms are the same.

206 GIOMAS can reproduce the asymmetry in the annual cycle of Antarctic SIV observed by ES and CS2

207 while underestimates SIV by about 38% on average when compared to ES as well as CS2. Meanwhile,

208 the underestimation is seasonally dependent, with weaker underestimation in summer and stronger one

209 in winter.

210 Figure 4 shows the spatial distribution of SIT bias in summer as well as winter to investigate details of

211 SIV underestimation in these two seasons. In both seasons, significant negative SIT bias of GIOMAS

212 can be found in the deformed ice zone, such as the northwestern Weddell Sea and coasts of the

213 Amundsen/Bellingshausen Sea as well as the coast of East Antarctic. Meanwhile, the extent of negative

214 bias is wider in the winter (Figs. 4b and d) rather than in the summer (Figs. 4a and c), which results in

215 seasonal differences of the SIV underestimation (Fig. 3). In addition, there are weakly positive SIT biases

216 in the southwestern Weddell Sea during winter (Figs. 4b and d), which may be due to model bias in

217 simulating sea-ice transport in the western Weddell Sea (Shi et al., 2021). Considering sea-ice

218 deformation is also related to sea-ice motion tightly, a better simulation of sea-ice motion is required to

219 achieve more accurate reconstruction of Antarctic SIT. In addition, the relatively large positive bias in

220 winter Ross Sea SIT can only be found in the comparison between GIOMAS and CS2, which may be

221 caused by smaller freeboard of CS2 than ES in the winter Ross Sea as shown in Paul et al. (2018). Notably,

222 some of the radar altimeter signals would originate from the snow/air interface or from somewhere inside

223 the snow and result in an overestimation of ice freeboard (Willatt et al., 2010; Wang et al., 2020).

224 These uncertainties, combined with often thick snow and complex snow metamorphism in the Antarctic,

225 can contribute to the overestimation of the Antarctic SIT from ES and CS2. Thus, the underestimation of

226 SIT from GIOMAS can be partially attributed to the uncertainties of SIT retrieved from ES and CS2.

227 However, the underestimation in the deformed ice regions can be owing to the deficiency of GIOMAS

228 since the differences of SIT between GIOMAS and satellite observations in those regions are always

229 larger than the uncertainties of satellite observations. To prove this, a direct inter-comparison between
230 the monthly SIT of GIOMAS, ES and ULS at site 206 is conducted and the biases of GIOMAS and ES
231 relative to ULS at site 206 and the uncertainties of each dataset are displayed in Table 1. The bias of
232 GIOMAS is larger than the uncertainty of ULS while the bias of ES is smaller than the uncertainty of
233 ULS (Tabel 1). This suggests there is a significant discrepancy between GIOMAS and ULS SIT while
234 ES SIT is comparable to ULS SIT at site 206.

235 Due to large uncertainties in above satellite observations, the SIT of GIOMAS is further assessed by ULS

236 measurement in the Weddell Sea. Considering significant variation of sea ice over horizontal distances

237 as small as a few meters, the standard deviation of ULS is displayed in Fig. 5a. It is obvious that the

238 variability of ULS near the shore (i.e., 206, 207, 212, 217, 232 and 233) is stronger than that of ULS far

239 from the shore (i.e., 208, 209, 210, 227, 229, 230 and 231), indicating larger sea-ice deformation near

240 the shore. As Fig. 5b shows, GIOMAS significantly underestimates the nearshore SIT all year round

241 while slightly overestimates SIT far from the shore in the winter, implying the deficiency of GIOMAS

242 in the simulation of sea-ice deformation, which leads to underestimation of SIT in the Weddell Sea from

243 a perspective of regional average. The above deficiency of GIOMAS might be attributed to the

244 insufficient resolutions of the model and assimilated SIC observations, which are not able to well resolve

245 the coastal lines and hinder GIOMAS from reproducing the ice deformation near shore. Therefore,

246 GIOMAS is indeed to underestimate the climatology of Antarctic SIT, mainly in the deformed sea-ice

247 zone, compared with satellite and in situ observations. In addition to the model drawbacks of GIOMAS,

248 this underestimation might also be introduced by the assimilation procedure of GIOMAS. Although only

249 satellite SIC is nudged in GIOMAS, SIT would be adjusted asymmetrically as described in Sect 2.1. This

250 asymmetric addition and removal of ice leads to a thinning of the mean ice thickness (Lindsay and Zhang,

251 2006). Notably, though the uncertainty of satellite observations is large, the differences between

252 GIOMAS and satellite SIT cannot be ignored since the uncertainty of satellite observations is expected

253 to be large owing to the difficulties with the estimation of snow depth and density in the Antarctic (Ozsoy-

254 Cicek et al., 2011; Bunzel et al., 2018).

255 **3.2   Comparison in the trend of SIV**

256 Antarctic SIE shows different trends before and after 2014 (Parkinson, 2019). Though there can be a

257 significant correlation between Antarctic SIE and SIV, differences between the variation of SIV and SIE

258 cannot be ignored in some regions. Therefore, it is necessary to examine whether there are similar

259 changes in the trend of Antarctic SIV. As Figure 6 shows, the observed Antarctic SIV anomaly increased

260 gradually from 2003, reached the maximum (2783 km^3) in November 2013, and then abruptly declined

261 from September 2013 to April 2017. The evolution of SIV anomaly is comparable to that of SIE anomaly,

262 while the time of the SIV anomaly peak is earlier than that of the SIE anomaly peak nearly by one year.

263 The trends of GIOMAS and observed SIV anomalies are 989 and 2968 km^3 per month before 2013 and

264 -84762 and -119875 km^3 per month after 2013. Although there are differences in the SIV trend between

265 GIOMAS and satellite observation, GIOMAS can basically reproduce the changes in the observed SIV

266 trend before and after 2013. Besides, the correlation of SIV anomalies between GIOMAS and

267 observations is 0.83, which passes a two-tailed t test at 99% significant level. Given the advantages of

268 reanalyses over observations or models individually especially in the polar region (Buehner et al., 2017),

269 GIOMAS data would be a good choice to study the variability and long-term trends of Antarctic sea ice.

270 **3.3   Comparison in the intensity of SIT variability**

271 Figure 7 displays spatial differences in the intensity of SIT anomalies variability between GIOMAS and

272 satellite observations. Compared with ES and CS2, GIOMAS underestimates the intensity of SIT

273 variability in the Southern Ocean, especially in the deformed ice zone (Figs. 7a-b), which resembles the

274 spatial pattern of Fig. 4. The underestimation in the deformed ice regions can be found also in the

275 comparison between GIOMAS and ULS. The intensity of SIT variability is underestimated near the shore,

276 while overestimated away from the shore (Fig. 7c). The spatial distribution of differences in the intensity

277 of variability is roughly consistent with that of SIT differences in Fig. 5b. These phenomena suggest that

278 there appears to be a relationship between the mean SIT and the variability. As Blanchard-Wrigglesworth

279 and Bitz (2014) suggested, models with a thinner mean ice state tend to have SIT anomalies with smaller

280 amplitude. In addition, the comparison in SIT standard deviation ratio and mean bias between GIOMAS

281 and satellite observations shown in supplementary figure further clarifies the relationship that with a

282 negative SIT bias, GIOMAS always underestimates the variability of SIT. Thus, the bias of SIT has an

283 impact not only on the climatology of SIT but also on the variability of SIT. It should be mentioned that

284 in the regions where the uncertainty of satellite observations is larger than the difference between

285 GIOMAS and satellite observations (i.e., mainly in the regions with undeformed sea ice), the uncertainty

286 would have an impact on the evaluation in the variability of SIT and cannot be ignored.

3.4 Comparison of SIT frequency

In addition to ULS observations, the rest of in situ sea-ice observations are sparse in the Southern Ocean and mainly provided by ship-based and air-based measurements. Figure 8 displays the SIT frequency distribution of GIOMAS and ship-based as well as air-based in situ observations. The peaks of observations are mainly around 0-0.6 m while the frequencies of GIOMAS SIT are mainly distributed in 0-1.4 m in the Southern Ocean (Fig. 8a). In different sectors (Figs. 8b-f), the frequency distribution of observed SIT data is similar to that in the whole Southern Ocean while the peaks of GIOMAS SIT frequency vary from 0.2 m to 1.4 m. Compared with observations, for the Southern Ocean, GIOMAS has a higher frequency within 0.6-1.6 m while a lower frequency in the rest bins compared with ship-based observations (Fig. 8a), which seems to imply the overestimation of SIT. The similar results can be found in different sectors (Figs. 8b-f). However, the sample selection bias should be noted in the ship-based observations due to ship's track avoiding areas of thicker ice, which results in its estimation biased toward thinner ice (Timmermann, 2004; Williams et al., 2015). Besides, GIOMAS has a lower frequency of thick ice in the Weddell Sea compared with air-based observations. In conclusion, GIOMAS tends to overestimate SIT frequency between 0.6-1.6 m in the Southern Ocean compared with ship-based observations under the premise that ship-based observations always bias low. Additionally, the comparison between GIOMAS and air-based SIT observations further proves the weakness of GIOMAS in the simulation of sea-ice deformation.

4 Conclusions and discussion

Considering the important role of SIT in studies of Antarctic sea ice and the wide application of GIOMAS, the Antarctic SIT of GIOMAS is assessed with satellite and in situ observations. In general, GIOMAS can basically reproduce the observed variability and linear trends of SIV even though only satellite SIC data is assimilated by nudging. For the climatology, GIOMAS can reproduce the asymmetry in the annual cycle of Antarctic SIV. For the long-term SIV variation, the variation of GIOMAS is in phase with that of observations, and it is also able to capture the changes in linear trends before and after 2013. These suggest that GIOMAS is useful to study the long-term variation of Antarctic sea ice. However, significant negative bias in SIT can be found in the comparison between of GIOMAS and observations. Compared with satellite measurements, GIOMAS tends to underestimate SIT, especially in regions with strong ice

315 deformation. This underestimation is of seasonal dependence with greater underestimation in the winter.

316 Although above underestimation can be partially attributed to the uncertainties of SIT retrieved from

317 satellite especially in the undeformed ice zone, the differences cannot be ignored and SIT

318 underestimation in the northwest Weddell Sea is further verified by the comparison between GIOMAS

319 and ULS observations. Furthermore, the spatial distribution of the differences in the magnitude of SIT

320 variability resembles that of the differences in SIT climatology between GIOMAS and observations.

321 Given the relationship between mean state of SIT and variability (Blanchard-Wrigglesworth and Bitz,

322 2014; also verified by the comparison between satellite observations and GIOMAS in the supplement),

323 this phenomenon indicates that SIT underestimation might have an impact on not only the SIT

324 climatology but also the SIT variability. In addition, GIOMAS overestimates SIT compared with ship-

325 based observations, which can be due to the negative bias in ship-based SIT estimation (Timmermann,

326 2004; Williams et al., 2015). The deficiency of GIOMAS in simulating deformed sea ice is further

327 verified in the comparison with air-based observations.

328 Notably, though GIOMAS could basically reproduce the trends of Antarctic SIV anomalies before and

329 after 2013, the differences in the trends of SIV anomalies between GIOMAS and satellite observations

330 cannot be ignored. A simple comparison between the monthly GIOMAS sea-surface temperature (SST)

331 and Microwave Optimally Interpolated SST observations reveals that the positive bias of GIOMAS in

332 SST before 2014 is roughly corresponding to the underestimation of positive trend of observed SIV

333 anomalies while the negative SST bias of GIOMAS after 2014 is corresponding to the underestimation

334 of negative trend of observed SIV anomalies. There seems to be a possible relationship between the

335 difference in SST and the difference in the trends of SIV anomalies between GIOMAS and observations

336 since higher SST would slow down the increase of SIV while lower SST would slow down the decrease

337 of SIV. However, this relationship needs further quantification and further analysis is added to our future

338 work plan.

339 In addition, limitations from Antarctic SIT observations are non-negligible in this study. For one aspect,

340 the scarcity of Antarctic SIT observations is one of the main sources of limitations for the evaluation.

341 The time span of satellite observations is not long enough for the evaluation of GIOMAS SIT data from

342 1979 to the present while the in situ observations are too few to show the estimation of SIT in the entire

343 Southern Ocean. Those make it unable to comprehensively evaluate the entire GIOMAS Antarctic SIT

344 data in this study. For another, this study is also limited by observations of Antarctic SIT due to their

345   unsuitability for the evaluation. For example, though SIT from ICESat (Kern et al., 2016) equipped with

346   the Geoscience Laser Altimeter System is available from 2004 to 2008 and proved to have lower bias in

347   SIT estimation than radar altimeter measurements (Willatt et al., 2010; Wang et al., 2020), it is not

348   adopted in this study. The reasons are as follows. First, ICESat SIT is not available in winter (July-

349   September), when greater underestimation of SIT is found in GIOMAS (Fig. 3). Second, the data size of

350   ICESat is relatively smaller than that of ES and CS2 because ICESat provides seasonal mean data and

351   its time range is narrower. Therefore, the additional assessment on SIT of GIOMAS will be conducted

352   when the Antarctic SIT derived from ICESat-2 is available. Furthermore, the uncertainty of satellite

353   observations has an impact on the evaluation and the accuracy of satellite observations needs to be further

354   improved to obtain more accurate satellite-derived SIT estimations with smaller uncertainty. The

355   uncertainty of satellite-derived SIT observations is mainly from the uncertainty introduced by the

356   scattering surface of radar signals and the estimation of Antarctic snow depth and density. With the

357   influences of complex snow stratigraphy and flooding inside the snow related to the formation of snow

358   ice, the assumption that the radar signal reflects from the snow/ice interface is not applicable in most

359   cases (Willatt et al., 2010). Besides, owing to the lack of knowledge of Antarctic snow, the climatology

360   of snow depth from the European Space Agency-SICCI Advanced Microwave Scanning Radiometer for

361   the Earth Observing System (AMSR-E) and the Advanced Microwave Scanning Radiometer 2 (AMSR2)

362   is used in the retrieval of ES and CS2-derived SIT, which would introduce extra uncertainties since the

363   inter-annual variability in snow depth is omitted (Bunzel et al., 2018). Moreover, the AMSR-E/AMSR2

364   snow depth is indicated to considerably underestimate the actual snow depth, which usually occurs in

365   the East Antarctic (Worby et al., 2008b; Ozsoy-Cicek et al., 2011). All those contribute to the large

366   uncertainty of the satellite-derived SIT in the Antarctic and the uncertainty would influence the

367   evaluation of SIT in the regions where the differences between GIOMAS SIT and satellite observations

368   are smaller than the uncertainty. Therefore, a more accurate estimation of Antarctic snow depth and

369   density would be essential to reducing the uncertainty of satellite SIT observations and thus improving

370   the reliability of the evaluation.

371   The above SIT underestimation of GIOMAS can be partially attributed to the model weakness. For

372   example, insufficient resolution of the model restricts GIOMAS to reproduce the ice deformation near

373   shore. Besides, the assimilation is a vital component in the reanalyses since it could constraint the model

374   with observations and make the model obtain better state estimation (Lahoz and Schneider, 2014).

375 However, it can also be a source of errors in the system. In GIOMAS, the asymmetric SIT changes

376 introduced by assimilation cannot be ignored. Thus, besides the further development of the model, there

377 are potential ways to improve the estimation of Antarctic SIT from the perspective of data assimilation.

378 Firstly, additional sea-ice observations other than SIC should be assimilated. For example, besides

379 Antarctic SIT derived from Envisat and CryoSat-2 used in this study, the Antarctic SIT retrieved from

380 ICESat-2 is also to be released in the near future, and hence assimilating these SIT observations directly

381 may suppress the bias of SIT (e.g., Yang et al., 2014; Fritzner et al., 2019; Luo et al., 2021). Also,

382 assimilating sea-ice drift observations can improve the simulation of sea-ice motion and deformation,

383 which can improve the estimation of SIT (e.g., Lindsay and Zhang, 2006; Mu et al., 2020). Secondly,

384 advanced data assimilation methods should be adopted to provide balanced estimation of model state.

385 For instance, the innovation of SIC can be converted to the increment of SIT in a more balanced way

386 through the flow-dependent covariance of Ensemble Kalman Filter (e.g., Massonnet et al., 2013; Yang

387 et al., 2015). Thirdly, due to the characteristics of SIC observations derived from the passive microwave

388 instrument, observation errors of SIC should vary with time and location (Lindsay and Zhang, 2006).

389 However, a fixed value of observation errors is adopted in GIOMAS because of limited information on

390 observation errors of SIC. Thus, a better estimation of SIC observation errors might further improve the

391 performance of GIOMAS. Furthermore, though nudging of SIC is not state of the art, it makes the model

392 of GIOMAS obtain better SIT simulation while the model only data of GIOMAS is likely to overestimate

393 SIT in the marginal seas. To promote the development of GIOMAS, further quantitative analyses on the

394 impact of nudging SIC on the SIT in the Antarctic are worthy of attention and will be conducted in the

395 future.

396 Besides, in the course of global warming, Antarctic SIE rose gradually and reached a record high in

397 2014/2015 before decreasing dramatically, which is obviously different from the dramatic drop in Arctic

398 SIE during the satellite era (e.g., Turner and Comiso, 2017). Results from a recent study suggest that the

399 trend in Antarctic ice coverage may be due to changes in atmospheric (e.g., Holland and Kwok, 2012)

400 and oceanic (e.g., Meehl et al., 2019) processes. Without better SIT and SIV estimates, it is difficult to

401 characterize how Antarctic sea-ice cover is responding to changing climate, or which climate parameters

402 are most influential (Vaughan et al., 2013). Thus, more Antarctic sea-ice observations and more studies

403 on data assimilation are urgently needed to accurately evaluate the Antarctic SIT, which can help to

404 improve the reconstruction and prediction of Antarctic SIV and to support research related to Antarctic

405   sea ice.

406   **Data availability**

407   The GIOMAS reanalysis data are available at
408   http://psc.apl.washington.edu/zhang/Global_seaice/data.html. The satellite-based Antarctic sea ice
409   thickness observations from Envisat and CryoSat-2 are available at
410   https://doi.org/10.5285/b1f1ac03077b4aa784c5a413a2210bf5 and
411   https://doi.org/10.5285/48fc3d1e8ada405c8486ada522dae9e8, respectively. The Weddell Sea upward-
412   looking sonar sea ice draft data are available at https://doi.pangaea.de/10.1594/PANGAEA.785565. The
413   ship-based sea ice thickness observations are available at http://aspect.antarctica.gov.au/data,
414   https://doi.org/10.1594/PANGAEA.819540 and https://doi.org/10.1594/PANGAEA.831976. The sea ice
415   thickness observations from airborne electromagnetic system are freely available at
416   https://doi.pangaea.de/10.1594/PANGAEA.771229 and https://epic.awi.de/id/eprint/36245/.

417   **Author contribution**

418   QY and HL developed the concept of the paper. SL and HL performed analysis and drafted the manuscript.
419   JW collected the remote sensing and observation data. QY, JZ, QS and JW gave comments and helped
420   revise the manuscript. All of the coauthors contributed to scientific interpretations.

421   **Competing interests**

422   The authors declare that they have no conflict of interest.

423   **Acknowledgments**

430 **References**

431 Abernathey, R. P., Cerovecki, I., Holland, P. R., Newsom, E., Mazloff, M., and Talley, L. D.: Water-
432 mass transformation by sea ice in the upper branch of the Southern Ocean overturning, Nat. Geosci., 9,
433 596-601, https://doi.org/10.1038/ngeo2749, 2016.

434 Alexandrov, V., Sandven, S., Wahlin, J., and Johannessen, O. M.: The relation between sea ice thickness
435 and freeboard in the Arctic, The Cryosphere, 4, 373-380, https://doi.org/10.5194/tc-4-373-2010, 2010.

436 Behrendt, A., Dierking, W., Fahrbach, E., and Witte, H.: Sea ice draft in the Weddell Sea, measured by
437 upward looking sonars, Earth Syst. Sci. Data, 5, 209-226, https://doi.org/10.5194/essd-5-209-2013, 2013.

438 Blanchard-Wrigglesworth, E., and Bitz, C. M.: Characteristics of Arctic Sea-Ice Thickness Variability
439 in GCMs, J. Climate, 27, 8244-8258, https://doi.org/10.1175/jcli-d-14-00345.1, 2014.

440 Buehner, M., Bertino, L., Caya, A., Heimbach, P., and Smith, G.: Sea Ice Data Assimilation, in: Sea Ice
441 Analysis and Forecasting: Towards an Increased Reliance on Automated Prediction Systems, edited by:
442 Lemieux, J.-F., Toudal Pedersen, L., Buehner, M., and Carrieres, T., Cambridge University Press,
443 Cambridge, 51-108, https://doi.org/10.1017/9781108277600.005, 2017.

444 Bunzel, F., Notz, D., and Pedersen, L. T.: Retrievals of Arctic Sea-Ice Volume and Its Trend Significantly
445 Affected by Interannual Snow Variability, Geophysical Research Letters, 45, 11,751-711,759,
446 https://doi.org/10.1029/2018GL078867, 2018.

447 Bushuk, M., Winton, M., Haumann, F. A., Delworth, T., Lu, F., Zhang, Y., Jia, L., Zhang, L., Cooke,
448 W., Harrison, M., Hurlin, B., Johnson, N. C., Kapnick, S., McHugh, C., Murakami, H., Rosati, A., Tseng,
449 K.-C., Wittenberg, A. T., Yang, X., and Zeng, F.: Seasonal prediction and predictability of regional
450 Antarctic sea ice, J. Climate, 1-68, https://doi.org/10.1175/jcli-d-20-0965.1, 2021.

451 Dahood, A., Watters, G. M., and de Mutsert, K.: Using sea-ice to calibrate a dynamic trophic model for
452 the Western Antarctic Peninsula, PloS One, 14, e0214814, https://doi.org/10.1371/journal.pone.0214814,
453 2019.

454 DuVivier, A. K., Holland, M. M., Kay, J. E., Tilmes, S., Gettelman, A., and Bailey, D. A.: Arctic and
455 Antarctic Sea Ice Mean State in the Community Earth System Model Version 2 and the Influence of
456 Atmospheric Chemistry, J. Geophys. Res.-Oceans, 125, e2019JC015934,
457 https://doi.org/10.1029/2019JC015934, 2020.

458 Fritzner, S., Graversen, R., Christensen, K. H., Rostosky, P., and Wang, K.: Impact of assimilating sea
459 ice concentration, sea ice thickness and snow depth in a coupled ocean–sea ice modelling system, The
460 Cryosphere, 13, 491-509, https://doi.org/10.5194/tc-13-491-2019, 2019.

461 Goosse, H., and Zunz, V.: Decadal trends in the Antarctic sea ice extent ultimately controlled by ice–
462 ocean feedback, The Cryosphere, 8, 453-470, https://doi.org/10.5194/tc-8-453-2014, 2014.

463 Harms, S., Fahrbach, E., and Strass, V. H.: Sea ice transports in the Weddell Sea, J. Geophy. Res.-Oceans,
464 106, 9057-9073, https://doi.org/10.1029/1999jc000027, 2001.

465 Haumann, F. A., Gruber, N., Münnich, M., Frenger, I., and Kern, S.: Sea-ice transport driving Southern
466 Ocean salinity and its recent trends, Nature, 537, 89-92, https://doi.org/10.1038/nature19101, 2016.

467 Hendricks, S., Paul, S., and Rinne, E.: ESA Sea Ice Climate Change Initiative (Sea_Ice_cci): Southern
468 hemisphere sea ice thickness from the CryoSat-2 satellite on a monthly grid (L3C), v2.0, Centre for
469 Environmental Data Analysis, https://doi.org/10.5285/48fc3d1e8ada405c8486ada522dae9e8, 2018a.

470 Hendricks, S., Paul, S., and Rinne, E.: ESA Sea Ice Climate Change Initiative (Sea_Ice_cci): Southern
471 hemisphere sea ice thickness from the Envisat satellite on a monthly grid (L3C), v2.0,
472 https://doi.org/10.5285/b1f1ac03077b4aa784c5a413a2210bf5, 2018b.

473 Hobbs, W. R., Massom, R., Stammerjohn, S., Reid, P., Williams, G., and Meier, W.: A review of recent
474 changes in Southern Ocean sea ice, their drivers and forcings, Global Planet. Change, 143, 228-250,
475 https://doi.org/10.1016/j.gloplacha.2016.06.008, 2016.

476 Holland, P. R., and Kwok, R.: Wind-driven trends in Antarctic sea-ice drift, Nat. Geosci., 5, 872-875,
477 https://doi.org/10.1038/ngeo1627, 2012.

478 Holland, P. R., Bruneau, N., Enright, C., Losch, M., Kurtz, N. T., and Kwok, R.: Modeled Trends in
479 Antarctic Sea Ice Thickness, J. Climate, 27, 3784-3801, https://doi.org/10.1175/jcli-d-13-00301.1, 2014.

480 Kalnay, E., Kanamitsu, M., Kistler, R., Collins, W., Deaven, D., Gandin, L., Iredell, M., Saha, S., White,
481 G., Woollen, J., Zhu, Y., Chelliah, M., Ebisuzaki, W., Higgins, W., Janowiak, J., Mo, K. C., Ropelewski,
482 C., Wang, J., Leetmaa, A., Reynolds, R., Jenne, R., and Joseph, D.: The NCEP/NCAR 40-year reanalysis
483 project,   B.   Am.   Meteorol.   Soc.,   77,   437-471,   https://doi.org/10.1175/1520-
484 0477(1996)077<0437:tnyrp>2.0.co;2, 1996.

485 Janjić, T., Bormann, N., Bocquet, M., Carton, J. A., Cohn, S. E., Dance, S. L., Losa, S. N., Nichols, N.
486 K., Potthast, R., Waller, J. A., and Weston, P.: On the representation error in data assimilation, Quarterly
487 Journal of the Royal Meteorological Society, 144, 1257-1278, https://doi.org/10.1002/qj.3130, 2018.

488 Kern, S., Ozsoy-Çiçek, B., and Worby, A.: Antarctic Sea-Ice Thickness Retrieval from ICESat: Inter-
489 Comparison of Different Approaches, Remote Sens.-Basel, 8, https://doi.org/10.3390/rs8070538, 2016.

490 Kumar, A., Dwivedi, S., and Rajak, D. R.: Ocean sea-ice modelling in the Southern Ocean around Indian
491 Antarctic stations, Journal of Earth System Science, 126, 70, https://doi.org/10.1007/s12040-017-0848-
492 5, 2017.

493 Kurtz, N. T. and Markus, T.: Satellite observations of Antarctic sea ice thickness and volume, Journal of
494 Geophysical Research: Oceans, 117, https://doi.org/10.1029/2012JC008141, 2012.

495 Lahoz, W. A. and Schneider, P.: Data assimilation: making sense of Earth Observation, Frontiers in
496 Environmental Science, 2, 10.3389/fenvs.2014.00016, 2014.

497 Lemke, P.: The Expedition of the Research Vessel Polarstern to the Antarctic in 2006 (ANT-XXIII/7),
498 Alfred-Wegener-Institut für Polar- und Meeresforschung;, Bremerhaven, Germany1866-3192, 1-147,
499 2009.

500 Lemke, P.: The Expedition of the Research Vessel Polarstern to the Antarctic in 2013 (ANT-XXIX/6),
501 Alfred-Wegener-Institut, Helmholtz-Zentrum für Polar- und Meeresforschung;, Bremerhaven,
502 Germany1866-3192, 1-154, 2014.

503 Lindsay, R. W., and Zhang, J.: Assimilation of ice concentration in an ice–ocean model, J. Atmos. Ocean.
504 Tech., 23, 742-749, https://doi.org/10.1175/jtech1871.1, 2006.

505 Luo, H., Yang, Q., Mu, L., Tian-Kunze, X., Nerger, L., Mazloff, M., Kaleschke, L., and Chen, D.:
506 DASSO: a data assimilation system for the Southern Ocean that utilizes both sea-ice concentration and
507 thickness observations, J. Glaciol., 1-6, https://doi.org/10.1017/jog.2021.57, 2021.

508 Maksym, T., and Markus, T.: Antarctic sea ice thickness and snow-to-ice conversion from atmospheric
509 reanalysis   and   passive   microwave   snow   depth,   J.   Geophys.   Res.,   113,
510 https://doi.org/10.1029/2006jc004085, 2008.

511 Maksym, T., Stammerjohn, S., Ackley, S., and Massom, R.: Antarctic Sea Ice—A Polar Opposite?,
512 Oceanography, 25, 140-151, https://doi.org/10.5670/oceanog.2012.88, 2012.

513 Massom, R. A., and Stammerjohn, S. E.: Antarctic sea ice change and variability – Physical and
514 ecological implications, Polar Sci., 4, 149-186, https://doi.org/10.1016/j.polar.2010.05.001, 2010.

Massom, R. A., Scambos, T. A., Bennetts, L. G., Reid, P., Squire, V. A., and Stammerjohn, S. E.: Antarctic ice shelf disintegration triggered by sea ice loss and ocean swell, Nature, 558, 383-389, https://doi.org/10.1038/s41586-018-0212-1, 2018.

Massonnet, F., Mathiot, P., Fichefet, T., Goosse, H., Beatty, C. K., Vancoppenolle, M., and Lavergne, T.: A model reconstruction of the Antarctic sea ice thickness and volume changes over 1980-2008 using data assimilation, Ocean Model., 64, 67-75, https://doi.org/10.1016/j.ocemod.2013.01.003, 2013.

Meehl, G. A., Arblaster, J. M., Chung, C. T. Y., Holland, M. M., DuVivier, A., Thompson, L., Yang, D., and Bitz, C. M.: Sustained ocean changes contributed to sudden Antarctic sea ice retreat in late 2016, Nat. Commun., 10, 14, https://doi.org/10.1038/s41467-018-07865-9, 2019.

Mishra, P., Alok, S., Rajak, D. R., Beg, J. M., Bahuguna, I. M., and Talati, I.: Investigating optimum ship route in the Antarctic in presence of sea ice and wind resistances – A case study between Bharati and Maitri, Polar Sci., https://doi.org/10.1016/j.polar.2021.100696, 2021.

Morioka, Y., Iovino, D., Cipollone, A., Masina, S., and Behera, S. K.: Summertime sea-ice prediction in the Weddell Sea improved by sea-ice thickness initialization, Sci. Rep.-UK, 11, 11475, https://doi.org/10.1038/s41598-021-91042-4, 2021.

Mu, L., Nerger, L., Tang, Q., Loza, S. N., Sidorenko, D., Wang, Q., Semmler, T., Zampieri, L., Losch, M., and Goessling, H. F.: Toward a data assimilation system for seamless sea ice prediction based on the AWI climate model, J. Adv. Model. Earth. Sy., 12, e2019MS001937, https://doi.org/10.1029/2019ms001937, 2020.

Ordoñez, A. C., Bitz, C. M., and Blanchard-Wrigglesworth, E.: Processes controlling Arctic and Antarctic sea ice predictability in the Community Earth System Model, J. Climate, 31, 9771-9786, https://doi.org/10.1175/jcli-d-18-0348.1, 2018.

Ozsoy-Cicek, B., Kern, S., Ackley, S. F., Xie, H., and Tekeli, A. E.: Intercomparisons of Antarctic sea ice types from visual ship, RADARSAT-1 SAR, Envisat ASAR, QuikSCAT, and AMSR-E satellite observations in the Bellingshausen Sea, Deep Sea Research Part II: Topical Studies in Oceanography, 58, 1092-1111, https://doi.org/10.1016/j.dsr2.2010.10.031, 2011.

Parker, W. S.: Reanalyses and observations: What's the difference?, B. Am. Meteorol. Soc., 97, 1565-1572, https://doi.org/10.1175/bams-d-14-00226.1, 2016.

Parkinson, C. L., and Cavalieri, D. J.: Antarctic sea ice variability and trends, 1979–2010, The Cryosphere, 6, 871-880, https://doi.org/10.5194/tc-6-871-2012, 2012.

Parkinson, C. L.: A 40-y record reveals gradual Antarctic sea ice increases followed by decreases at rates far exceeding the rates seen in the Arctic, P. Natl. Acad. Sci. USA, 116, 14414-14423, https://doi.org/10.1073/pnas.1906556116, 2019.

Parrinello, T., Shepherd, A., Bouffard, J., Badessi, S., Casal, T., Davidson, M., Fornari, M., Maestroni, E., and Scagliola, M.: CryoSat: ESA's ice mission – Eight years in space, Adv. Space Res., 62, 1178-1190, https://doi.org/10.1016/j.asr.2018.04.014, 2018.

Paul, S., Hendricks, S., Ricker, R., Kern, S., and Rinne, E.: Empirical parametrization of Envisat freeboard retrieval of Arctic and Antarctic sea ice based on CryoSat-2: progress in the ESA Climate Change Initiative, The Cryosphere, 12, 2437-2460, https://doi.org/10.5194/tc-12-2437-2018, 2018.

Ricker, R.: Sea ice conditions during POLARSTERN cruise ANT-XXIX/7, PANGAEA, https://doi.org/10.1594/PANGAEA.831976, 2016.

Robel, A. A.: Thinning sea ice weakens buttressing force of iceberg mélange and promotes calving, Nat. Commun., 8, 14596, https://doi.org/10.1038/ncomms14596, 2017.

558   Rollenhagen, K., Timmermann, R., Janjić, T., Schröter, J., and Danilov, S.: Assimilation of sea ice
559   motion in a finite-element sea ice model, J. Geophys. Res., 114, https://doi.org/10.1029/2008jc005067,
560   2009.

561   Schultz, C.: Antarctic sea ice thickness affects algae populations, Eos Trans. AGU, 94, 40-40,
562   https://doi.org/10.1002/2013EO030032, 2013.

563   Schwegmann, S.: Sea ice conditions during POLARSTERN cruise ANT-XXIX/6 (AWECS),
564   PANGAEA, https://doi.org/10.1594/PANGAEA.819540, 2013.

565   Shi, Q., Yang, Q., Mu, L., Wang, J., Massonnet, F., and Mazloff, M. R.: Evaluation of sea-ice thickness
566   from four reanalyses in the Antarctic Weddell Sea, The Cryosphere, 15, 31-47,
567   https://doi.org/10.5194/tc-15-31-2021, 2021.

568   Shu, Q., Song, Z.-Y., and Qiao, F.-L.: Assessment of sea ice simulations in the CMIP5 models, The
569   Cryosphere, 9, 399-409, https://doi.org/10.5194/tc-9-399-2015, 2015.

570   Timmermann, R.: Utilizing the ASPeCt sea ice thickness data set to evaluate a global coupled sea ice–
571   ocean model, J. Geophys. Res., 109, https://doi.org/10.1029/2003jc002242, 2004.

572   Tsujino, H., Urakawa, L. S., Griffies, S. M., Danabasoglu, G., Adcroft, A. J., Amaral, A. E., Arsouze, T.,
573   Bentsen, M., Bernardello, R., Böning, C. W., Bozec, A., Chassignet, E. P., Danilov, S., Dussin, R.,
574   Exarchou, E., Fogli, P. G., Fox-Kemper, B., Guo, C., Ilicak, M., Iovino, D., Kim, W. M., Koldunov, N.,
575   Lapin, V., Li, Y., Lin, P., Lindsay, K., Liu, H., Long, M. C., Komuro, Y., Marsland, S. J., Masina, S.,
576   Nummelin, A., Rieck, J. K., Ruprich-Robert, Y., Scheinert, M., Sicardi, V., Sidorenko, D., Suzuki, T.,
577   Tatebe, H., Wang, Q., Yeager, S. G., and Yu, Z.: Evaluation of global ocean–sea-ice model simulations
578   based on the experimental protocols of the Ocean Model Intercomparison Project phase 2 (OMIP-2),
579   Geosci. Model Dev., 13, 3643-3708, https://doi.org/10.5194/gmd-13-3643-2020, 2020.

580   Turner, J., Hosking, J. S., Bracegirdle, T. J., Marshall, G. J., and Phillips, T.: Recent changes in Antarctic
581   Sea Ice, Philos. Trans. A Math. Phys. Eng. Sci., 373, https://doi.org/10.1098/rsta.2014.0163, 2015.

582   Turner, J., and Comiso, J.: Solve Antarctica's sea-ice puzzle, Nature, 547, 275-277,
583   https://doi.org/10.1038/547275a, 2017.

584   Uotila, P., Iovino, D., Vancoppenolle, M., Lensu, M., and Rousset, C.: Comparing sea ice, hydrography
585   and circulation between NEMO3.6 LIM3 and LIM2, Geosci. Model Dev., 10, 1009-1031,
586   https://doi.org/10.5194/gmd-10-1009-2017, 2017.

587   Uotila, P., Goosse, H., Haines, K., Chevallier, M., Barthélemy, A., Bricaud, C., Carton, J., Fučkar, N.,
588   Garric, G., Iovino, D., Kauker, F., Korhonen, M., Lien, V. S., Marnela, M., Massonnet, F., Mignac, D.,
589   Peterson, K. A., Sadikni, R., Shi, L., Tietsche, S., Toyoda, T., Xie, J., and Zhang, Z.: An assessment of
590   ten ocean reanalyses in the polar regions, Clim. Dyn., 52, 1613-1650, https://doi.org/10.1007/s00382-
591   018-4242-z, 2019.

592   Vaughan, D. G., Comiso, J. C., Allison, I., Carrasco, J., Kaser, G., Kwok, R., Mote, P., Murray, T., Paul,
593   F., Ren, J.-W., E. Rignot, E., Solomina, O., Steffen, K., and Zhang, T.-J.: Observations: Cryosphere, in:
594   Climate change 2013: The physical science basis. Contribution of working group I to the fifth assessment
595   report of the intergovernmental panel on climate change, edited by: Stocker, T. F., Qin, D.-H., Plattner,
596   G.-K., Tignor, M., Allen, S. K., Boschung, J., Nauels, A., Xia, Y., Bex, V., and Midgley, P. M.,
597   Cambridge University Press, Cambridge, United Kingdom and New York, NY, USA, 317-382,
598   https://doi.org/10.1017/CBO9781107415324.012, 2013.

599   Wang, J., Min, C., Ricker, R., Yang, Q., Shi, Q., Han, B., and Hendricks, S.: A comparison between
600   Envisat and ICESat sea ice thickness in the Antarctic, The Cryosphere Discuss., 2020, 1-26,
601   https://doi.org/10.5194/tc-2020-48, 2020.

602   Weaver, R., Morris, C., and Barry, R. G.: Passive microwave data for snow and ice research: Planned

603   products from the DMSP SSM/I System, Eos Trans. AGU, 68, 769-777,

604   https://doi.org/10.1029/EO068i039p00769, 1987.

605   Willatt, R. C., Giles, K. A., Laxon, S. W., Stone-Drake, L., and Worby, A. P.: Field Investigations of

606   Ku-Band Radar Penetration Into Snow Cover on Antarctic Sea Ice, IEEE T. Geosci. Remote, 48, 365-

607   372, https://doi.org/10.1109/TGRS.2009.2028237, 2010.

608   Williams, G., Maksym, T., Wilkinson, J., Kunz, C., Murphy, C., Kimball, P., and Singh, H.: Thick and

609   deformed Antarctic sea ice mapped with autonomous underwater vehicles, Nat. Geosci., 8, 61-67,

610   https://doi.org/10.1038/ngeo2299, 2015.

611   Worby, A. P., Geiger, C. A., Paget, M. J., Van Woert, M. L., Ackley, S. F., and DeLiberty, T. L.:

612   Thickness distribution of Antarctic sea ice, J. Geophys. Res.-Oceans, 113,

613   https://doi.org/10.1029/2007JC004254, 2008a.

614   Worby, A. P., Markus, T., Steer, A. D., Lytle, V. I., and Massom, R. A.: Evaluation of AMSR-E snow

615   depth product over East Antarctic sea ice using in situ measurements and aerial photography, Journal of

616   Geophysical Research: Oceans, 113, https://doi.org/10.1029/2007JC004181, 2008b.

617   Yang, Q., Losa, S. N., Losch, M., Tian-Kunze, X., Nerger, L., Liu, J., Kaleschke, L., and Zhang, Z.:

618   Assimilating SMOS sea ice thickness into a coupled ice-ocean model using a local SEIK filter, J.

619   Geophys. Res.-Oceans, 119, 6680-6692, https://doi.org/10.1002/2014jc009963, 2014.

620   Yang, Q., Losa, S. N., Losch, M., Liu, J., Zhang, Z., Nerger, L., and Yang, H.: Assimilating summer sea-

621   ice concentration into a coupled ice-ocean model using a LSEIK filter, Ann. Glaciol., 56, 38-44,

622   https://doi.org/10.3189/2015AoG69A740, 2015.

623   Zhang, J., and Rothrock, D. A.: Modeling global sea ice with a thickness and enthalpy distribution model

624   in generalized curvilinear coordinates, Mon. Weather Rev., 131, 845-861, https://doi.org/10.1175/1520-

625   0493(2003)131<0845:Mgsiwa>2.0.Co;2, 2003.

626   Zhang, J.: Increasing Antarctic Sea Ice under Warming Atmospheric and Oceanic Conditions, J. Climate,

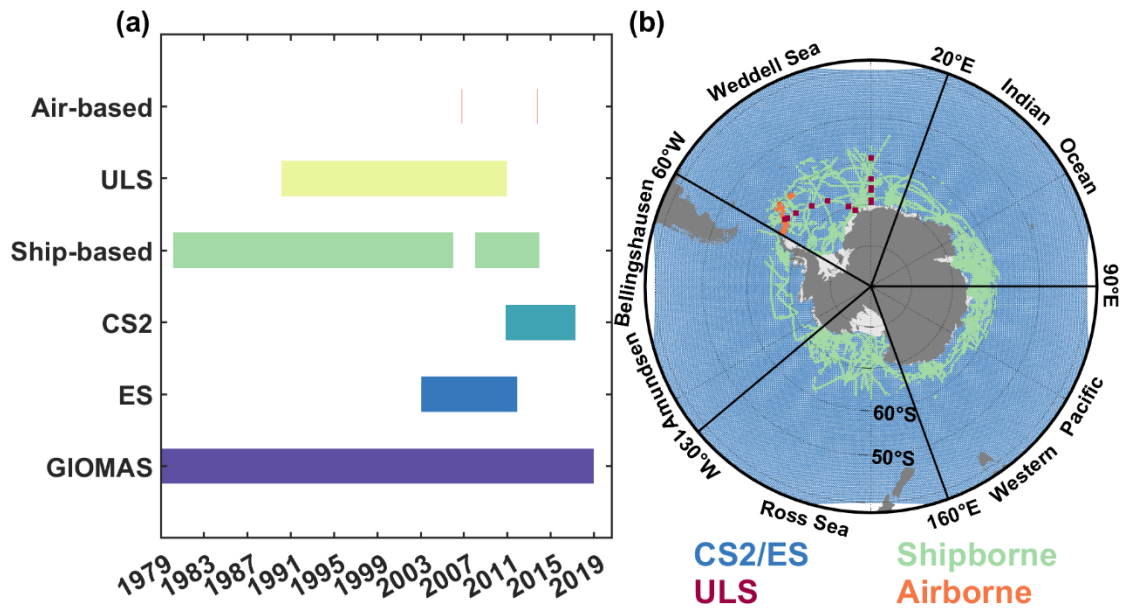627   20, 2515-2529, https://doi.org/10.1175/jcli4136.1, 2007.

628

629 **Table 1.** The biases of GIOMAS and ES SIT relative to that of ULS and the uncertainties of SIT at ULS
630 206 (Unit: m).

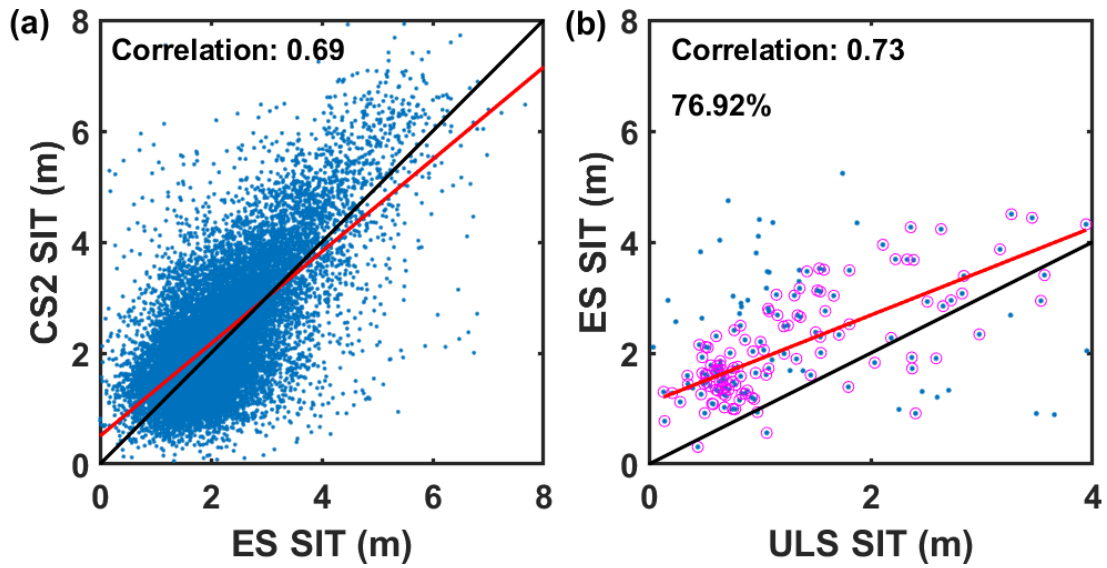| Dataset	Bias	Uncertainty
ULS	0	1.17
ES	0.89	1.37
GIOMAS	-1.99	0.34

631

632

633

634   **Figure 1.** (a) The temporal and (b) spatial coverage of data used in this study.
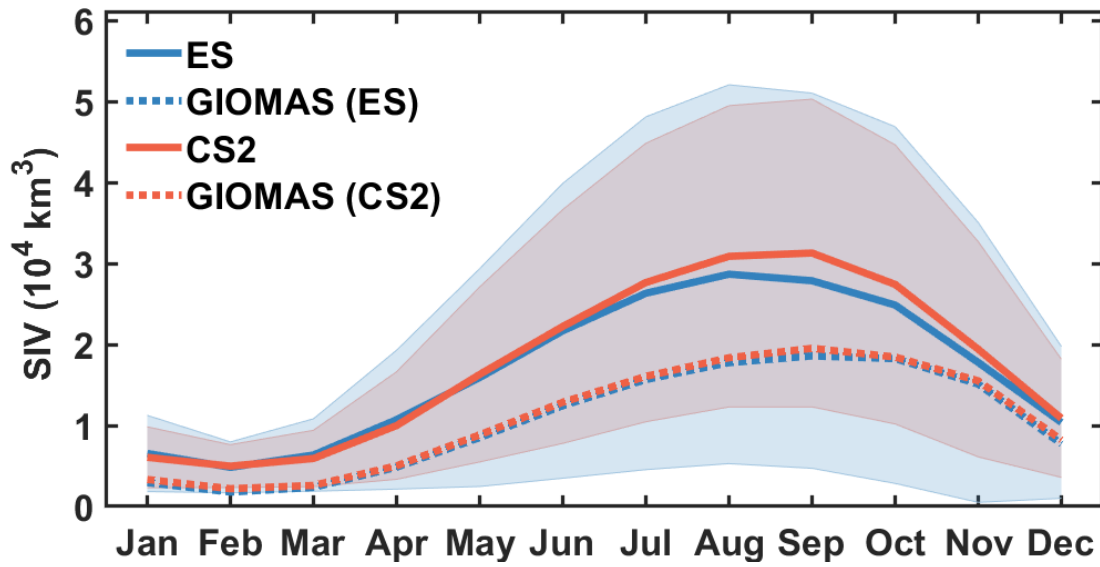
635

636

637

644

645

Figure 3. The climatological annual cycle of Antarctic SIV. The blue and red denote data related to ES

and CS2, respectively. The solid and dashed curves denote satellite observations and corresponding
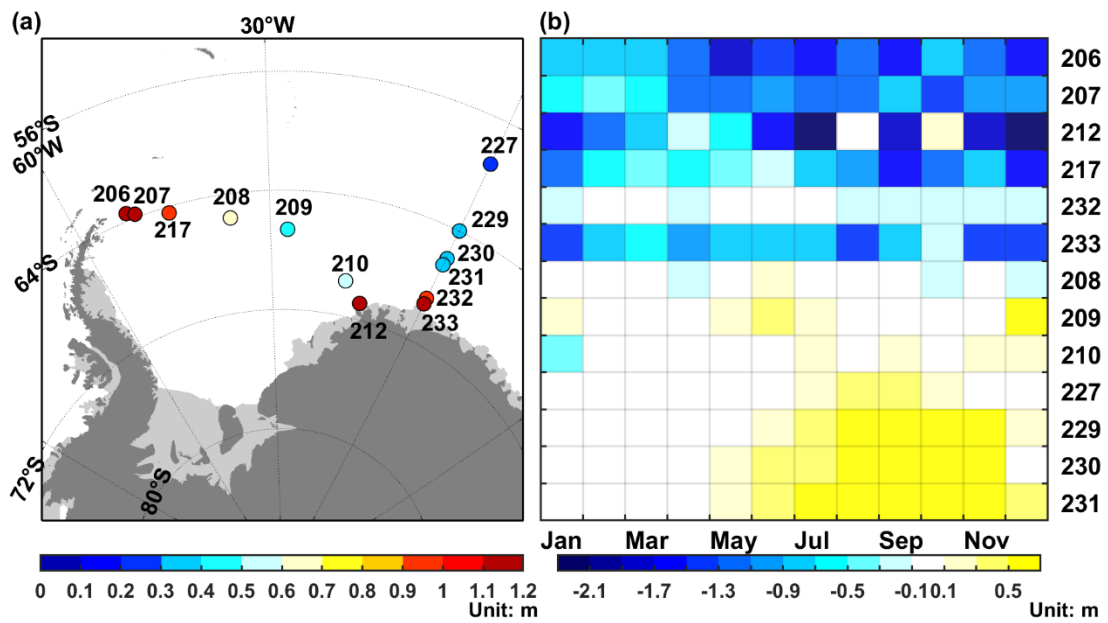
GIOMAS data.
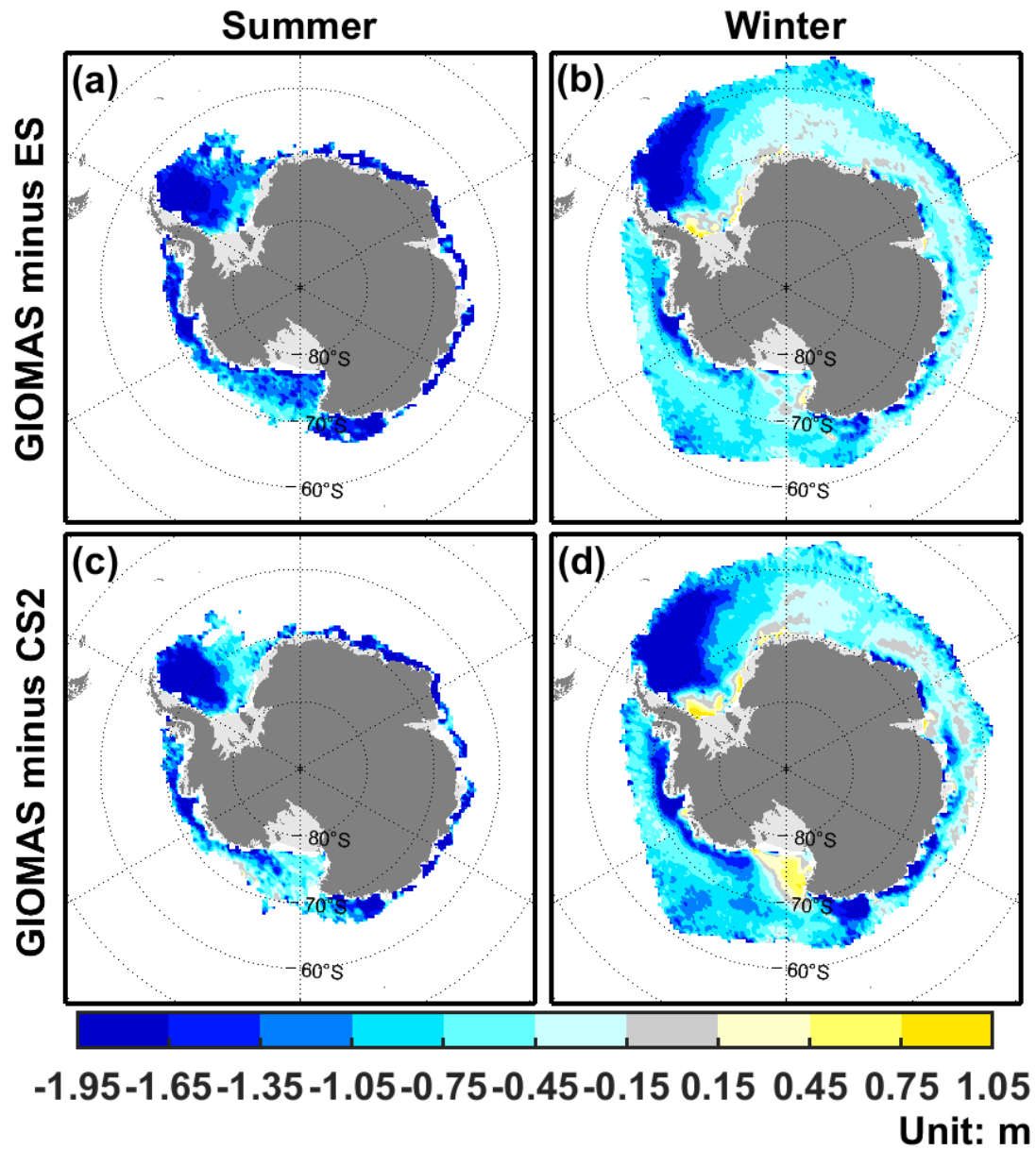
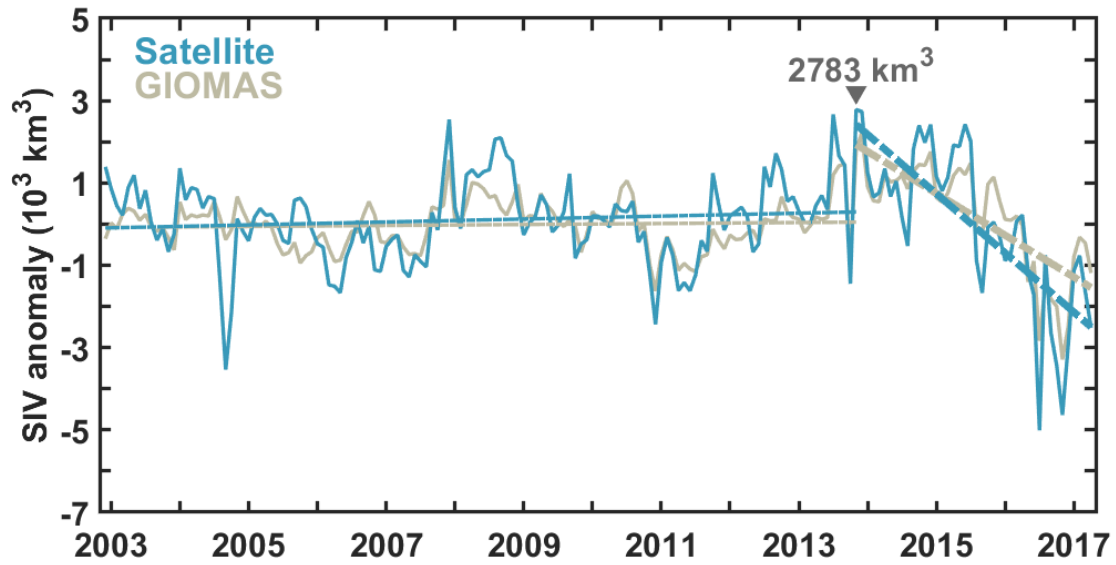**Figure 4.** The SIT bias of GIOMAS relative to ES in (a) the summer and (b) winter. (c-d) same as (a-b) but for bias relative to CS2.

Figure 5. (a) The locations of ULS in the Weddell Sea and corresponding standard deviation of SIT. (b) The differences in SIT climatology between GIOMAS and ULS.
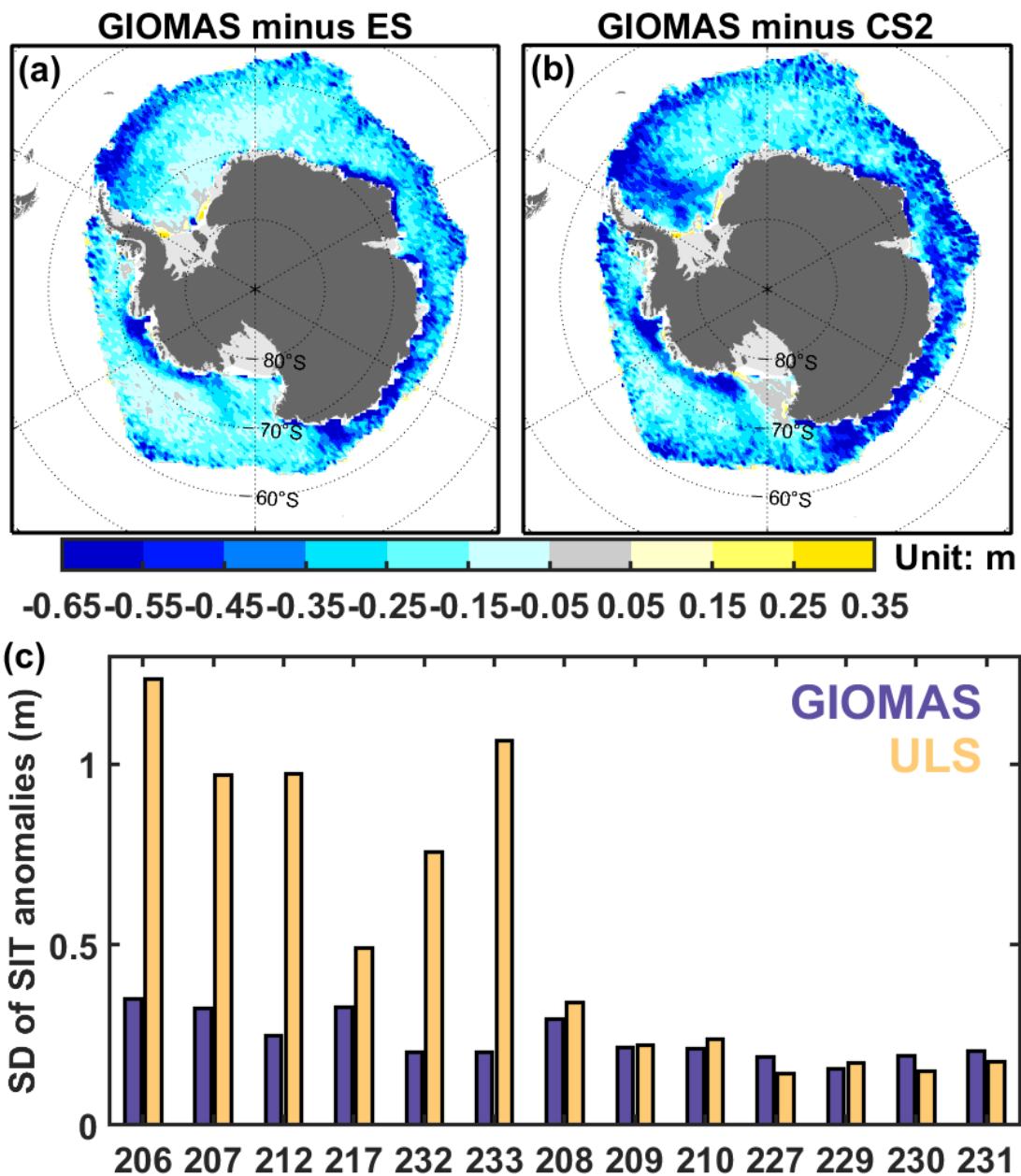
658

659 **Figure 6.** The SIV anomalies of satellite observations (green) and corresponding GIOMAS (khaki). The

660 dashed lines denote the linear trends of SIV anomalies from December 2002 to November 2013 and from

661 November 2013 to April 2017. All linear trends have passed a F-test at 99% significant level.

662

GIOMAS minus ES

GIOMAS minus CS2

(a)

(b)

Unit: m

-0.65 -0.55 -0.45 -0.35 -0.25 -0.15 -0.05 0.05 0.15 0.25 0.35

(c)

GIOMAS
ULS

206 207 212 217 232 233 208 209 210 227 229 230 231

663

Figure 7. (a) The spatial differences in standard deviation of SIT anomalies between GIOMAS and ES.
(b) same as (a) but for differences between GIOMAS and CS2. (c) The standard deviation of SIT
anomalies for ULS (yellow) and corresponding GIOMAS (blue).

667

668
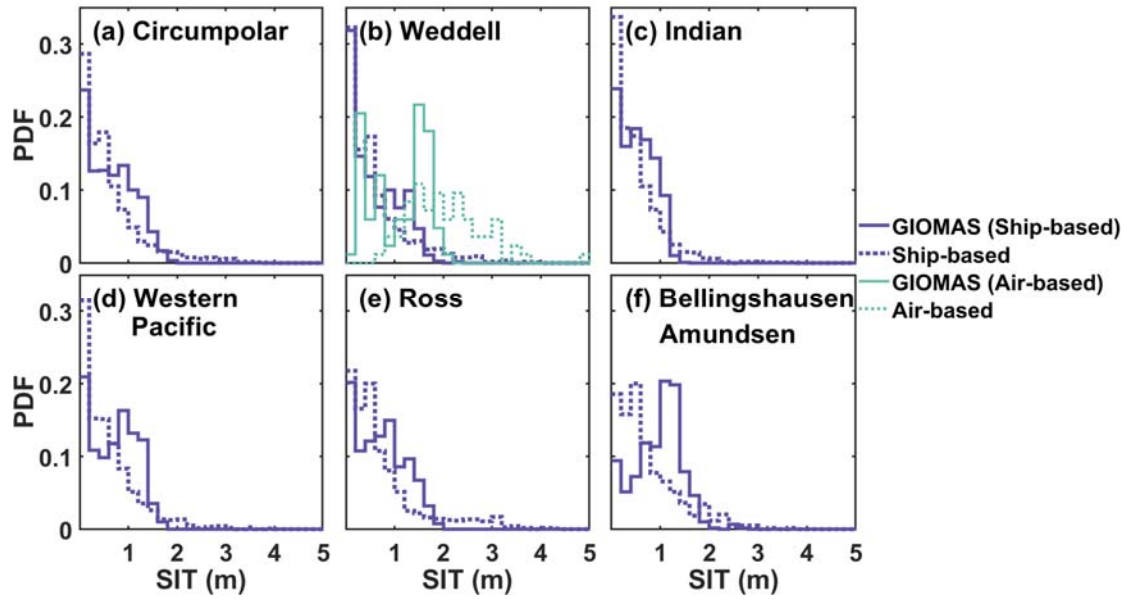
Figure 8. SIT histograms of GIOMAS and in situ observations in (a) the Southern Ocean and (b-f)

670   different sectors.